Journal of Surface Analysis Vol.20, No. 3 (2014) pp. 155−160
C. J. Powell New Data Resources and Applications for AES and XPS

Invited paper

New Data Resources and Applications for AES and XPS

C. J. Powell*
National Institute of Standards and Technology, Gaithersburg, Maryland 20899-8370, USA
*cedric.powell@nist.gov

(Received: November 11, 2013; Accepted: December 13, 2013)

A description is given of several new applications of the NIST Database for the Simulation of Electron Spectra for Surface Analysis (SESSA). These applications include: (i) the determination of effective attenuation lengths for different XPS configurations, algorithms, and materials; (ii) examination of the effects of elastic scattering on film thicknesses obtained from the Tougaard QUASES software; and (iii) estimation of XPS detection limits and amounts of material in samples with complex morphologies. An overview is also given of a recent evaluation of calculated and measured cross sections for inner-shell ionization by electron impact. New recommendations have been made for K-shell and L- and M-subshell ionization cross sections. These cross sections will be available in a new NIST database that is expected to be released in 2014.

1. Introduction

Auger-electron spectroscopy (AES), secondary-ion mass spectrometry (SIMS), and X-ray photoelectron spectroscopy (XPS) are in common use for surface analysis. Figure 1 shows the numbers of published AES, SIMS, and XPS papers published per year from 1991 through 2012 based on a key word search. Two sets of AES publication data are included in Fig. 1, one based on the use of 'AES' in the search and the other without this term. The former data set is an overcount (because AES is also an abbreviation for atomic emission spectroscopy), while the latter data set is an undercount (since some Auger papers with AES in the title or abstract would be missed). Nevertheless, it appears from Fig. 1 that the number of Auger papers is roughly constant or slowly decreasing while the number of SIMS papers is slowly increasing. There is a much larger growth in the number of XPS papers, probably due to the fact that XPS has been successfully applied to many different types of materials [2]. The plots in Fig. 1 do not, of course, show the many unpublished practical applications of each technique nor the economic impacts of these applications. Nevertheless, Fig. 1 indicates that XPS applications are of growing significance.

The National Institute of Standards and Technology (NIST) has six databases available for AES, XPS, and other applications [1]:

- NIST X-ray Photoelectron Spectroscopy Database (SRD 20)
- NIST Electron Elastic-Scattering Cross-Section Database (SRD 64)
- NIST Electron Inelastic-Mean-Free-Path Database (SRD 71)
- NIST Electron Effective-Attenuation-Length Database (SRD 82)
- NIST Database for the Simulation of Electron Spectra for Surface Analysis (SESSA) (SRD 100)
- NIST Backscattering-Correction-Factor Database for Auger Electron Spectroscopy (SRD 154)

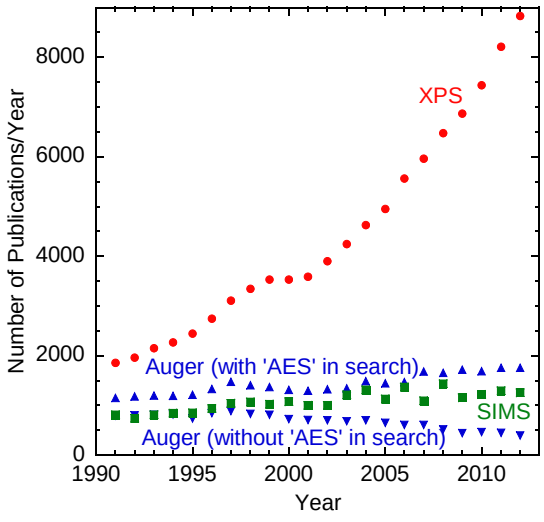

Fig. 1 Plot of numbers of papers published per year on AES, SIMS, and XPS from 1991 through 2012 based on a web search using abbreviations and key phrases for these techniques.

Critical reviews have been published describing evaluations of the data included in SRD 64 [2], SRD 71 [3], and SRD 82 [4], and a similar review of the data in SRD 154 is in preparation [5]. SRD 100 includes differential and total cross sections for elastic scattering of electrons and transport cross sections from SRD 64 as well as electron inelastic mean free paths from SRD 71. We note that the data in SRD 64, in particular, can be used for other applications such as electron-probe microanalysis (EPMA), electron-beam lithography, plasma physics, radiation processing, radiation therapy, and radiation dosimetry.

This article contains brief summaries of three new applications of the SESSA database (SRD 100) and of a new evaluation of measured and calculated cross sections for K-shell and L- and M-subshell ionization by electron impact [6]. The latter cross sections are relevant for quantitative applications of AES and EPMA, and are expected to be available in a new NIST database in 2014 (SRD 164).

2. New Applications of SESSA (SRD 100)

SESSA was designed to facilitate quantitative interpretations of AES and XPS spectra and to improve the accuracy of quantitation in routine analysis. SESSA contains the physical data needed to perform quantitative interpretation of an AES or XPS spectrum for a specimen of given composition. Retrieval of relevant data is performed by a small expert system that queries the comprehensive databases [7]. A simulation module provides an estimate of peak intensities as well as the energy and angular distributions of the emitted electron flux.

The current version of SESSA can provide simulated AES or XPS spectra for multi-layered thin films. The simulated spectra, for layer compositions and thicknesses specified by the user, can then be compared with measured spectra. The layer compositions and thicknesses can then be adjusted to find maximum consistency between simulated and measured spectra, as described in Section 2.3. A new version of SESSA that can simulate AES or XPS spectra for nanostructured materials (such as islands, lines, spheres, and layered spheres) is expected to be available in 2014.

2.1 Effective Attenuation Lengths for XPS

The effective attenuation length (EAL) has been defined by the International Organization for Standardization (ISO) as a parameter which, when introduced in place of the inelastic mean free path (IMFP) into an expression derived for AES or XPS on the assumption that elastic-scattering effects are negligible for a given quantitative application, will correct that expression for elastic-scattering effects [8]. The EAL is a parameter that is commonly used for determining the thicknesses of overlayer films by AES and XPS, but there are other applications [4]. That is, an EAL has to be defined and applied for a specific quantitative algorithm or application.

Powell *et al*. [9] used SESSA to simulate photoelectron intensities for thin films of $SiO_{1.6}N_{0.4}$ and $HfO_{1.9}N_{0.1}$ on silicon with excitation by Al Kα X-rays. They considered Si $2p_{3/2}$ photoelectrons from $SiO_{1.6}N_{0.4}$ and the substrate and Hf $4f_{7/2}$ photoelectrons from $HfO_{1.9}N_{0.1}$. The simulations were performed for ranges of film thicknesses and photoelectron emission angles and for two commonly used configurations for XPS, the sample-tilting configuration and the Theta Probe configuration.[1] They determined EALs by two methods, one by analyzing photoelectron intensities as a function of film thickness for each emission angle (Method 1) and the other by analyzing photoelectron intensities as a function of emission angle for each film thickness (Method 2). The analyses were made with simple expressions that had been derived with the assumption that elastic-scattering effects were negligible. They found that EALs from both methods were systematically larger for the Theta Probe configuration, by amounts varying between 1 % and 5 %, than those for the sample-tilting configuration. These differences were attributed to anisotropy effects in the photoionization cross section that are expected to occur in the former configuration. Generally similar EALs were found by each method for each film material although larger EALs were found from Method 2 for film thicknesses less than 1.5 nm.

SESSA is thus a useful tool for showing how elastic

[1] Certain commercial products are identified to specify experimental conditions or software. These identifications do not imply that the products are endorsed or recommended by the National Institute of Standards and Technology, or that they are necessarily the most suitable for the purpose described.

scattering of photoelectrons modifies EALs for particular materials, film thicknesses, and XPS configurations.

2.2 Sample-Morphology Effects on XPS Peak Intensities

It has long been known that variations in sample morphology can have drastic effects on photoelectron intensities in XPS [10]. Morphological parameters such as crystallinity, roughness, and island or grain dimensions can modify peak intensities and their associated inelastic tails. We will consider here photoelectron spectra and peak intensities from several sample morphologies in which the composition of an element of interest is varying with depth. For example, the intensity of a substrate photoelectron line will change considerably following deposition of an overlayer film of increasing thickness. It is therefore generally necessary for an analyst to deduce the morphology of the sample of interest before attempting a quantitative analysis [10]. Alternatively, the sample morphology might be known or can reasonably be inferred from the prior history of the sample, particular processing steps (e.g., deposition of a film), or knowledge gained from similar samples.

Two examples will be given of the use of SESSA for obtaining more quantitative information from XPS spectra of thin-film samples.

2.2.1 Effects of Elastic Scattering on Film Thicknesses Determined by the Tougaard QUASES Software[1]

In a seminal 1996 paper, Tougaard [11] showed model spectra with identical Cu $2p_{3/2}$ XPS peak intensities that were obtained from four Cu/Au samples with very different morphologies: a 2.5 nm Au film on a Cu substrate, a 1 nm Cu buried film in an Au matrix, a 5 nm $CuAu_4$ alloy on an Au substrate, and a thin Cu film on an Au substrate. Although the peak Cu $2p_{3/2}$ intensities were the same for each morphology, the samples had very different distributions of copper concentration versus depth and very different amounts of copper in the near-surface region of each sample. An XPS analysis based solely on the Cu $2p_{3/2}$ peak intensity and the assumption of a homogeneous sample would thus yield an incorrect result for these Cu/Au morphologies. Tougaard also showed that the shapes of the inelastic spectra on the low-energy side of the $2p_{3/2}$ peak for each morphology were very different. With use of an algorithm for photoelectron transport in the solid, analysis of the XPS peak shape (i.e., the main or no-loss peak and its accompanying inelastic region) could give information on the depth distribution of the emitting atom and the amount of that substance. Tougaard developed convenient software, named QUASES,[1] for this purpose [12].

The Tougaard algorithm and software are based on the assumption that elastic scattering of the detected photoelectrons can be neglected. Powell *et al*. [13] have employed SESSA to test this assumption for two classes of materials, two XPS configurations, and two conditions, one in which elastic scattering is neglected (corresponding to the Tougaard results) and the other in which it is included. They considered the Cu/Au morphologies analyzed by Tougaard and similar SiO_2/Si morphologies since elastic-scattering effects are expected to be smaller in the latter materials than the former materials.

Film thicknesses in the simulations were adjusted in each case to give essentially the same chosen Cu $2p_{3/2}$ or O 1s peak intensity. Film thicknesses with elastic scattering switched on were systematically less than those with elastic scattering switched off by up to about 25 % for the Cu/Au morphologies and up to about 14 % for the SiO_2/Si morphologies. For the two morphologies in which the Cu $2p_{3/2}$ or O 1s peak intensity was attenuated by an overlayer, the ratios of film thicknesses with elastic scattering switched on to those with elastic scattering switched off varied approximately linearly with the single-scattering albedo, a convenient measure of the strength of elastic scattering. This variation was similar to that of the ratio of the EAL to the IMFP for the photoelectrons in the overlayer film. For the two morphologies in which the Cu $2p_{3/2}$ or O 1s photoelectrons originated from an overlayer film, the ratios of film thicknesses with elastic scattering switched on to those with elastic scattering switched off varied more weakly with the single-scattering albedo. This weaker variation was attributed to the weaker effects of elastic scattering for photoelectrons originating predominantly from near-surface atoms than for photoelectrons that travel through an overlayer film.

These SESSA simulations showed how film thicknesses determined from the Tougaard QUASES software could be corrected for the effects of elastic scattering.

2.2.2 Detection Limits in XPS

Early XPS experiments showed, for example, that fractional monolayers (MLs) of an adsorbate could be detected [14]. These experiments indicated that XPS detection limits typically varied between 0.1 and 1 atomic per cent. Nevertheless, it has often been difficult in many practical applications to quantify detection limits and amounts of material in XPS analyses of samples with complex morphologies. Brief summaries will now be given of two illustrative applications of SESSA to determine XPS detection limits and amounts of material for a sample consisting of a surface layer or for a buried thin film in a substrate.

In the first example [15], SESSA simulations were made to compare the peak intensity for a weak peak from a minor element in a sample (e.g., from a surface layer on a substrate or from a buried thin film in a matrix) with the *same intensity* of that element assumed to be homogeneously distributed in the particular substrate or matrix. That is, the amount of a dilute element of known concentration in a homogeneous matrix material at or near the XPS detection limit could be related to the amount of that element present as a surface layer or a buried thin film.

Simulations were made for a $RuW_{0.001}$ alloy, a thin W film of thickness *t* on a Ru substrate, and W films of varying thicknesses, *t*, buried at various depths, *z*, in a Ru matrix. For the $RuW_{0.001}$ alloy, the ratio of the intensity of the W $4d_{5/2}$ peak to the Ru $3d_{5/2}$ peak was 1.25×10^{-3}, and it was assumed that this represented the smallest amount of W that could be detected in a Ru matrix. In the following simulations for the surface W film and the buried W layers, the thickness *t* was varied for each chosen *z* to obtain the same W $4d_{5/2}$ peak intensity (within 1 %) as that found for the $RuW_{0.001}$ alloy. These thicknesses varied from about 0.006 ML for $z = 0$ to about 4 ML for $z/\lambda = 4$ where λ is the IMFP of the W $4d_{5/2}$ photoelectrons in Ru. These SESSA simulations thus indicated the likely XPS detection limits for W films in or on Ru.

In the second example [16], SESSA simulations were made of the XPS spectra for prototype multilayer mirrors (MLMs) intended for use in extreme ultraviolet lithography. The MLMs typically consist of 40 to 60 pairs of Si-Mo films on a Si substrate capped by a Ru layer, and are engineered to give high reflectivity at a wavelength of 13.5 nm (92 eV). After exposure to wafer processing conditions (e.g., various outgassing products), the MLMs often have surface species present (e.g., C, F, S, and P) that can degrade the reflectivity. XPS is often used to detect these surface species and to estimate their concentrations. These estimates are generally based on a simplified approach in which it is assumed that the sample is homogeneous. It has proven difficult, however, to make meaningful comparisons of these estimated compositions from one XPS laboratory to another since different XPS instruments were used (with different configurations, operating conditions, and software systems).

The SESSA simulations [16] showed that the intensity of a weak Cl peak in the XPS spectrum of a test MLM corresponded to a 0.5 nm surface C layer containing about 0.02 ML of Cl. SESSA can thus be used as a tool to quantify the amount of impurities (or other minor elements) present in particular layers of a multilayered thin-film structure. Properties of the structure such as reflectivity can then be meaningfully correlated with the derived impurity concentration.

3. Cross Sections for Ionization of Inner-Shell Electrons by Electron Impact

A new evaluation has been made of measured and calculated cross sections for K-shell and L- and M- subshell ionization by electron impact [6]. These cross sections are often expressed in terms of the overvoltage, *U*, the ratio of the incident energy to the binding energy of the shell or subshell of interest. Bote and Salvat [17] showed that cross-section calculations could be made with the plane-wave Born approximation for overvoltages greater than 16 and with the distorted-wave Born approximation for lower overvoltages. This approach is very attractive since the calculations can be made for any neutral atom and for a wide range of incident electron energies. K-shell and L- and M-subshell ionization cross sections were calculated by this method for all atoms from hydrogen to einsteinium from the ionization threshold to 1 GeV. These cross sections were fitted to two analytical formulae by Bote *et al*. [18], one for $U \leq 16$ and the other for $U \geq 16$.

Llovet *et al*. [6] made graphical comparisons of available measurements of K-shell and L- and M-subshell ionization cross sections with the corresponding cross sections from the Bote *et al*. [18] formulae. Similar comparisons were made of measured Lα X-ray produc-

tion cross sections and values obtained from the L_3-subshell ionization cross sections and the needed relaxation data from the Evaluated Atomic Data Library [19]. Llovet *et al.* identified elements for which there were at least three (for K shells) or two (for L and M subshells) mutually consistent sets of cross-section measurements and for which there was satisfactory agreement with the energy dependence expected from theory (the Bote *et al*. cross sections). Use of the calculated cross sections was critical in the evaluation because consistency (or otherwise) could be established for sets of data in non-overlapping energy ranges.

Llovet *et al*. identified 26 elements with sets of measured K-shell ionization cross sections that satisfied their selection criteria. The percentage deviations of these cross sections from the Bote *et al*. calculated cross sections did not vary significantly with overvoltages between 1.02 and 2×10^5, and the average values of these deviations did not vary significantly with atomic number from $Z = 6$ to $Z = 83$. The average root-mean-square (RMS) deviation between the measured and corresponding calculated cross sections was 10.3 %, while the average deviation was -1.9 %.

In similar comparisons, seven elements were identified that satisfied the evaluation criteria for total L-shell ionization cross sections and one element for which there were two sets of L_3-subshell ionization cross-section measurements. The average RMS deviation between the measured and corresponding calculated cross sections was 15.0 % while the average deviation was -3.1 %.

Three elements were found for which there were two or more sets of M-shell ionization cross sections that satisfied the evaluation criteria. The average RMS deviation between the measured and corresponding calculated cross sections was 23.5 % while the average deviation was 8.2 %.

Eight elements were identified for which there were two or more sets of measured Lα X-ray production cross sections that satisfied the evaluation criteria. The average RMS deviation between the measured and corresponding calculated cross sections was 10.6 % while the average deviation was -7.3 %.

The overall average RMS deviation between the measured and corresponding calculated cross sections was 10.9 % and the overall average deviation was -2.5 %. This degree of agreement between measured and calculated ionization and X-ray production sections was considered very satisfactory given the difficulties of making absolute cross-section measurements. Larger deviations were found between the measured L- and M-subshell ionization cross sections and the corresponding calculated values than for the K-shell cross sections. This result was not unexpected because of the additional uncertainties associated with the needed atomic data [19].

Llovet *et al.* [6] also made comparisons of K-shell, L_3-subshell, and M_5-subshell ionization cross sections from the analytical formulae of Gryzinski [20], Casnati *et al*. [21], Jakoby *et al*. [22], and Hombourger [23] for selected elements with those from the Bote *et al*. formulae. They found that K-shell and L_3-subshell ionization cross sections from the Casnati *et al*. and Hombouger formulae agreed satisfactorily with the corresponding Bote *et al*. cross sections but there was poorer agreement for the M_5-subshell cross sections. There were much larger deviations between cross sections from the Gryzinski and Jakoby *et al.* formulae and those from the Bote *et al*. formulae.

NIST is planning to release a new database (SRD 164) containing cross sections for K-shell and L- and M-subshell ionization by summer, 2014. These cross sections will be based on the formulae of Bote *et al*. [18] that were evaluated by Llovet *et al*. [6].

4. Summary

The NIST SESSA database is a useful tool for quantitative applications of AES and XPS. Three new applications of SESSA were described: (i) determination of effective attenuation lengths (needed for measurements of overlayer film thicknesses) for different XPS analysis methods and different XPS configurations; (ii) correction for elastic-scattering effects of film thicknesses obtained from the Tougaard QUASES software; and (iii) estimation of detection limits in XPS and amounts of particular species in samples with complex morphologies. A new version of SESSA for simulations with nanostructures is expected in 2014.

A comprehensive evaluation has been made of measured and new calculations of cross sections for ionization of K shells and of L and M subshells by electron impact. Superior data were identified that showed ≈ 11 % consistency with the calculated cross sections. A new NIST database with K-shell and L- and M-subshell ionization

cross sections is expected to be released in 2014.

5. Acknowledgments

The work described here has been carried out in collaboration with W. S. M. Werner, W. Smekal, G. Tasneem, S. Tougaard, N. Faradzhev, S. B. Hill, X. Llovet, F. Salvat, and A. Jablonski.

6. References

[1] http://www.nist.gov/srd/surface.cfm.

[2] A. Jablonski, F. Salvat, and C. J. Powell, *J. Phys. Chem. Ref. Data* **33**, 409 (2004).

[3] C. J. Powell and A. Jablonski, *J. Phys. Chem. Ref. Data* **28**, 19 (1999).

[4] A. Jablonski and C. J. Powell, *Surf. Science Reports* **47**, 33 (2002).

[5] A. Jablonski and C. J. Powell (to be published).

[6] X. Llovet, C. J. Powell, F. Salvat, and A. Jablonski, *J. Phys. Chem. Ref. Data* **43**, 013102 (2014).

[7] W. Smekal, W. S. M. Werner, and C. J. Powell, *Surf. Interface Anal.* **37**, 1059 (2005).

[8] ISO 18115-1, Surface chemical analysis – Vocabulary – Part 1: General Terms and terms used in spectroscopy, International Organization for Standardization (Geneva, 2010).

[9] C. J. Powell, W. S. M. Werner, W. Smekal, and G. Tasneem, *Surf. Interface Anal.* **45**, 628 (2013).

[10] C. J. Powell and A. Jablonski, *J. Electron Spectrosc. Relat. Phenom.* **178-179**, 331 (2010).

[11] S. Tougaard, *J. Vac. Sci. Technol. A* **14**, 1415 (1996).

[12] http://www.quases.com.

[13] C. J. Powell, S. Tougaard, W. S. M. Werner, and W. Smekal, *J. Vac. Sci. Technol. A* **31**, 021402 (2013).

[14] T. E. Madey, J. T. Yates, and N. E. Erickson, *Chem. Phys. Letters* **19**, 487 (1973).

[15] C. J. Powell, W. S. M. Werner, and W. Smekal (to be published).

[16] N. S. Faradzhev, S. B. Hill, and C. J. Powell (to be published).

[17] D. Bote and F. Salvat, *Phys. Rev. A* **77**, 042701 (2008).

[18] D. Bote, F. Salvat, A. Jablonski, and C. J. Powell, *At. Data. Nucl. Data Tables*, **96**, 871 (2009); *ibid*. **97**, 186 (2011).

[19] S. T. Perkins, D. E. Cullen, M. H. Chen, J. H. Hubbell, J. Rathkopf, and J. Scofield, Tables and graphs of atomic subshell and relaxation data derived from the LLNL evaluated atomic data library (EADL), *Z* = 1 – 100, Technical Report UCRL-ID-50400, Lawrence Livermore National Laboratory, Livermore, California, 1991.

[20] M. Gryzinski, *Phys. Rev.* **138**, A336 (1965).

[21] E. Casnati, A. Tartari, and C. Baraldi, *J. Phys. B: Atom. Mol. Phys.* **15**, 155 (1982); *ibid*. **16**, 505 (1983).

[22] C. Jakoby, H. Genz, and A. Richter, *J. Phys. (Paris) Colloq.* **48**, 487 (1987).

[23] C. Hombourger, *J. Phys. B: At. Mol. Opt. Phys*. **31**, 3693 (1998).